Journal of Nuclear Materials 523 (2019) 71–79

Contents lists available at ScienceDirect

Journal of Nuclear Materials

journal homepage: www.elsevier.com/locate/jnucmat

Hydrogen distribution induced screw dislocation core spreading in tungsten

Yinan Wang [a], Xiaoyang Wang [a], Xiaoyu Wu [a], Qiulin Li [a, b], Chengliang Li [c], Guogang Shu [c], Ben Xu [a, *], Wei Liu [a, **]

[a] Key Laboratory of Advanced Materials (MOE), School of Material Science and Engineering, Tsinghua University, Beijing, 100084, China
[b] Graduate School at Shenzhen, Tsinghua University, Shenzhen, China
[c] State Key Laboratory of Nuclear Power Safety Monitoring Technology and Equipment, China Nuclear Power Engineering Co., Ltd., Shenzhen, 518172, China

ARTICLE INFO

Article history:
Received 10 December 2018
Received in revised form
11 May 2019
Accepted 20 May 2019
Available online 23 May 2019

Keywords:
Dislocation structure
First-principle calculation
Molecular dynamics
Hydrogen
Surface energy

ABSTRACT

The underlying physical mechanisms of the retention and self-clustering of hydrogen(H) in tungsten(W) are important in understanding the radiation damage and plasma trapping of W-based components in divertors, in which the influence of dislocations has not been sufficiently addressed. For this purpose, quantum mechanics/molecular dynamics(QM/MD) simulations are performed to investigate the distribution of hydrogen(H) clusters along screw dislocation lines in W, where the spreading of the screw dislocation core is first observed introduced by the H clusters. This core spreading constitutes an essential factor that could account for the hydrogen embrittlement phenomenon.

1. Introduction

The rigorous challenge faced by modern energy production necessitates the research and development of thermonuclear fusion facilities. The materials in such facilities may serve in the extreme conditions, including the impact by heat fluxes, radiation, and plasma exposure. The properties of materials will be degraded during their services, which could also lead to penetration and trapping of plasma components including retention. With recent developments in the international thermonuclear experimental reactor (ITER), tungsten(W) is the most promising candidate for plasma facing components as the divertor and first wall, due to its high melting point, low erosion rates in cold scrape-off layer plasma, and low tritium retention [1–4]. During ITER service, W components are under the complex effect of thermal stresses, which is coupled with trapping of plasma components and irradiation damage. The damages related to hydrogen isotopes are induced by the retention of H by the W lattice and defects, leading to the formation of bubbles and their following-up growth into blisters. The understanding of fundamental physical mechanisms of H retention in the material would greatly facilitate the estimation of accumulation of hydrogen isotopes in W and the assessment of lifetime of such materials.

Many experimental efforts have been dedicated to the study of interaction of H isotopes with W under ITER-relevant exposure conditions [5–8]. These results revealed that the retention of hydrogen plasma can severely damage the material stability. Furthermore, the accumulation of the hydrogen isotopes will deteriorate the mechanical properties of W, including the embrittlement and early crack formation.

The mechanical properties degradation of W components should be assessed under the consideration of the coupling effect of H isotopes and irradiation induced defects. Embrittlement is directly correlated with screw dislocation(SD) mobility, which is further determined by the core structure of such dislocations. Detailed *ab-initio* calculations were performed to explain the clustering properties of H in W and showed that H–H length smaller than 1.8 Å leads to strong repulsion, whereas for larger interaction distances, the binding energy is close to zero [9]. Unless induced by intrinsic or radiation-induced lattice defects, this DFT

* Corresponding author.
** Corresponding author.
E-mail addresses: xuben@mail.tsinghua.edu.cn (B. Xu), liuw@tsinghua.edu.cn (W. Liu).

https://doi.org/10.1016/j.jnucmat.2019.05.038
0022-3115/

simulation result excludes the possibility of the H self-clustering in tungsten [10]. Regarding the interaction between the H and screw dislocations in W, D. Terentyev et al. [11] demonstrated that H atoms interacted strongly with the screw dislocation core in body-centered cubic (bcc) W, while A. Bakaev et al. [12] studied the interaction of H and He atoms with edge dislocations(EDs) and screw dislocations to derive the interaction energy landscape. These studies have clarified that the dislocations could trap the H and He atoms strongly.

To date, few studies have focused on the structural change of SD cores induced by H solutes. The SD core structure significantly influences the mobility of the dislocations, and further, the macroscopic mechanical behavior of the W. In addition, the pipe distribution of H solutes in Fe along the SD line [13], which could be a reasonable retention form in W has also received limited attention. In this paper, we explore the interaction of hydrogen with the SD core. In the result part, we demonstrate that hydrogen atoms exhibit a one-dimensional (1D) distribution along the SD line at low concentrations using quantum mechanics/molecular dynamics(QM/MD) calculations [13]. Increasing the concentration of the hydrogen atoms results in the spreading of the SD core to an asymmetric structure. The concentration of the hydrogen solute in the dislocation core is estimated with the mean-field model. In the discussion part, two possible reasons for the core spreading phenomenon are considered. Firstly, the γ surface of tungsten with hydrogen permeation is calculated, which is a criterion [14–17]for determining whether the core is asymmetric or symmetric. Secondly, a study of the stress field of the SD core is carried out to clarify the increasing edge components as the main reason for dislocation spread.

2. Method of simulation

2.1. QM/MD method

In this work, the QM/MD [13] method is employed to determine the reasonable core structures of SDs in W and the distribution of the hydrogen atoms. In this work, molecular dynamics method is employed for the static simulations, so the name “molecular dynamics” is used instead of the original “molecular mechanics” in Zhao's paper for easily understand. In the QM/MD approach, the system is composed of two regions: the dislocation core region (I), which is surrounded by the rest of the areas(II). The total energy of the system can be expressed as $E_{tot} = E^{EAM}_{I,II} + E^{DFT}_{I} - E^{EAM}_{I}$, which is the energy of the entire system calculated by the embedded atom method (EAM) $E^{EAM}_{I,II}$, plus the DFT calculated energy of dislocation core region I E^{DFT}_{I}, minus the EAM calculated energy of region I E^{EAM}_{I}. The accuracy of the calculated structures is further enhanced by the introduction of a boundary region, B, around the dislocation core, which serves to reduce the coupling errors between EAM method and DFT method, and the force on the boundary DFT atoms is corrected as $F^{corr}_{i}[B] = -F^{DFT}_{i}[B] + F^{EAM}_{i}[B]$. Accordingly, the total energy in the revised coupling scheme is modified: $E^{mod}_{tot}[I + II] = E_{tot}[I + II] - \sum^{B}_{i} F^{corr}_{i}[B] \cdot u_i[B]$. The $u_i[B]$ is the displacement of the ith boundary atom at each relaxation step, and the sum is over all boundary atoms (B). The detailed description of the technique is provided in other references such as Ref. [13,18]. With the QM/MD algorithm, the dislocation core with solutes could be treated accurately by the QM method, regardless of the weak description of certain defects by the EAM potential of the MD method. The atomic structure of the crystal employed in the QM/MD simulation is displayed in Fig. 1. Different regions are handling with DFT or MD methods. Region I and the inner part of region B are dealing with DFT, while the outer part of region B and region II are handled by MD. To set up the input, SD core is established based on the theoretical displacement field. Then QM method is applied to describe the accurate SD core structure in region I, while the atoms in region B are held rigid as a buffer. As for the rest atoms in region II, the MD method is employed to minimize the total energy and the atomic forces. During this step, the atoms in region I and region B are not allowed to move. Then, the MD method is utilized on atoms in region B and the atoms in region I and II are immobilized. After finishing a cycle of the relaxation for all the regions, the convergence of total energy and the atomic force on each atom are checked. The accuracy of the QM/MD method is validated in our former work [18], that the core structure of the screw dislocation, the binding energy of H to the SD and to the edge dislocation are comparable with existing ab initio data [11,19].

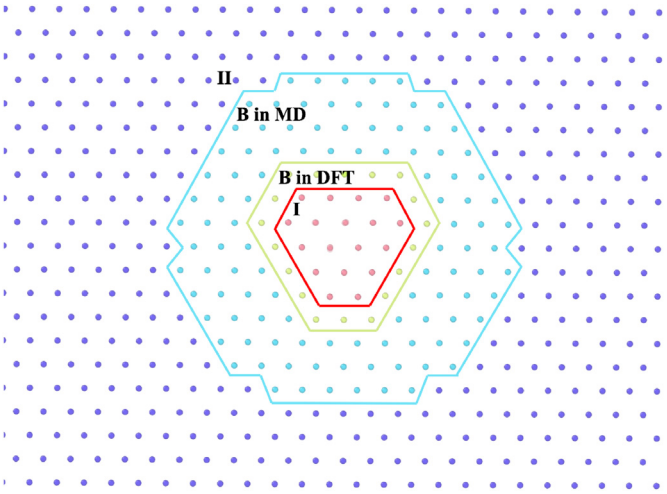

Fig. 1. The atomic structure of the crystal employed in the QM/MD simulation. The region I, B in DFT, B in MD and II in MD, highlighting in red, green, light blue and purple, respectively. (For interpretation of the references to color in this figure legend, the reader is referred to the Web version of this article.)

2.2. Dislocation model

In the simulation models of this study, the SD is placed at the center of a cubic box. The dislocation is created by displacing atoms according to the anisotropic elasticity theory of straight line defects [20]. In this study, it is an isolated SD with a Burgers vector along the Z axis, which is set to be a/2[11$\bar{1}$] and a is the lattice constant. The X, Y, and Z axes are aligned along the [112], [1$\bar{1}$0], and [11$\bar{1}$], respectively. 144 atoms are included in region I and region B for DFT simulations, where 76 inner atoms are considered region I and are dealt with the DFT method. 68 outer atoms are frozen during the DFT simulation, which are considered as region B. Besides, region B is enlarged to 564 atoms, while during the DFT simulation the outer atoms were not considered because the DFT method could work on a limited number of atoms. After preliminary test, both the SD core structure and its stress field could converge reasonably with these atom numbers. The periodic boundary condition is applied along the X [112] and Z [11$\bar{1}$] directions, while the Y [1$\bar{1}$0] boundary is set free. The total cell dimensions are 770, 770, and 11.05 Å along the X, Y, and Z directions, respectively, and the sizes along X, Y and Z for the DFT-treated region are 18, 18 and 11 Å. The size of the crystal along Z is 4b, where b is the Burgers vector.

2.3. Simulation details

The QM calculations are accomplished via the Vienna Ab initio Simulation Package (VASP) [21–23] within the spin-polarized

generalized gradient approximation (GGA) [24]. In the calculations, ultrasoft pseudopotentials are employed. To describe the interaction between ions and electrons, Blochs projector augmented-wave (PAW) [25] method is applied. For H, the 1s state is treated as valence state, while for W the valence state is selected as 5d6s state. The Monkhorst-Pack Scheme [26] is carried out to sample the Brillouin zone. In all situations, the k-points are chosen as $1 \times 1 \times 2$, and the plane wave cut-off energy was taken to be 350 eV in order to get converged results [9,27,28]. The energy convergence criterion for self-consistent reiteration is set 10^{-4} eV. All positions of atoms are fully optimized until the residual stresses are lower than 0.001 eV/Å. The MD calculations are conducted with the widely used LAMMPS code [29]. A semi-empirical embedded atom method (EAM) is applied for the MD simulations based on a potential developed by X. W. Zhou et al. [30]. The differences between the lattice constant and bulk modulus estimated by QM and MD methods are eliminated by scaling the EAM potential to such properties [31]. The geometry of SD is analyzed by a differential displacement map [32]. All the atomistic structures are visualized and are rendered by the Open Visualization Tool (ovito) [33].

3. Results

3.1. Binding energy

In this paper, the dislocation configurations with different concentrations of hydrogen atoms along the dislocation line and the $H_N - SD$ interaction are assessed, where N represents the number of hydrogen atoms and varies from 1 to 10. A column of hydrogen atoms with different N values is manually added to the energy-minimum sites [12] inside the SD core along the same column as the initial state. After relaxation, the hydrogen atoms will deviate from their original sites and find the energy minimum positions. The corresponding incremental binding energy of H with the SD is defined as $E^B_{D+NH} = E_{D+NH} - E_{D+(N-1)H} - E_{bulk+NH} + E_{bulk+(N-1)H}$, where N is the number of hydrogen atoms, E_{D+NH} is the total energy of the system when N hydrogen atoms are attached to the SD and $E_{bulk+NH}$ is the total energy of the bulk W system containing N hydrogen atoms. The H–H interaction is almost negligible since the elastic binding effect is compensated for by the change in effective position of the H states in the electronic structure [9]. In this relation, a negative binding energy corresponds to an attractive interaction between two objects [11]. The definition of the binding energy included the dislocation energy with (N-1) H atoms, from which the influence of the different number of H atoms clustering along the dislocation line could be revealed. The change of the incremental binding energy not only displayed the propensity for the H to form clusters at the dislocation core versus in bulk, but also presented the energy compensation of the core structure and the clustering shapes due to different concentrations of H. Since the interaction between the H atoms in W is repulsive according to former DFT simulations, so it is hard to estimate the clustering of the H atoms without the dislocations.

The incremental binding energy of hydrogen to the $H_{N-1} - SD$ complex is presented in Fig. 2 (a). All the energies are negative, suggesting that an increasing number of hydrogen atoms form a stable complex spreading along the dislocation line, and the H self-cluster could be induced by the SD line. The incremental binding energy rises from a minimum at N = 8, indicating that the spreading of the SD core decreases the energy of the whole system. Without hydrogen, the spreading core energy is 0.165 eV/b higher than the compact core, and this value is between the excess energy of the hard core and the split core as displayed in Table 2 of Ventelon's work [34]. The spreading core is not exactly the hard core or the split core, and it is less energetically favorable if there is no hydrogen. The physical origin of the increasing binding energy with the 8th hydrogen is that the relative stability of the different core structures is inverted by a high concentration of the hydrogen solutes. With the spreading of the dislocation core, the energy of the system is lowered and the dislocation could accommodate more hydrogen solutes. The error of the incremental binding energy resulting from the force correction is listed for different N in Fig. 2(b), which is around 10^{-4} eV to 10^{-3} eV. Overall, the SD line could act as a reasonable line defect to contain H solute atoms.

3.2. Low concentration of hydrogen solutes

For low concentrations of hydrogen solutes, the dislocation spreads isotropically along the six $<112>$ directions and exhibits an approximately threefold rotational point group symmetry about the $[11\bar{1}]$ axis through the center of the map. The SD core structure remains compact, which is called a non-degenerate core, as represented in Fig. 3(a). Introducing two hydrogen atoms into the SD core does not alter the core structure; the SD remains a nondegenerate, symmetric easy-core configuration [35], in agreement with various DFT calculations for W [17,36–38]. Two hydrogen atoms are located inside the SD core, which are slightly different from the energy minimum positions predicted by Bakaev [39]. In the work by Bakaev, only one hydrogen atom was considered in the interaction energy map, while the repulsion between two hydrogen atoms could account for the deviation of the energy minimum sites predicted in his work and our work. This result implies that when the limited hydrogen atoms are located in the SD core, they do not significantly disturb the core structure.

3.3. Spiral distribution of hydrogen solutes

In situations involving a greater number of hydrogen atoms in the SD core, the hydrogen atoms occupy energy-minimum interstitials and formed a spiral along the dislocation line, as shown in Fig. 3(b), which presents a differential displacement map of the core structure with 6 hydrogen atoms; the corresponding ball-and-stick model is presented in Fig. 3(d). In Fig. 3(b), only 3 H atoms could be observed because the other 3 H atoms are in the same positions from the view of $[11\bar{1}]$ direction. In Fig. 3(d), the other 3 H atoms have the same arrangement along the dislocation line, so only 3 of them are displayed as an example. The spiral shape of the distribution is similar to the path shape of the hydrogen atoms diffusing in the Fe SDs [13], where the pipe diffusion of hydrogen atoms along the dislocation line occurs through jumping between the adjacent energy-minimum interstitials. We also note that the SD core structure is not disturbed by such a concentration of the hydrogen atoms. When the number of hydrogen atoms does not reach 8, each hydrogen atom occupies an energy-minimum interstitial inside the core without disturbing the core structure. Thus, the saturation concentration of hydrogen in the SD core without core spreading is defined, that for every supercell with thickness of 2 Burger's vector, 3 is the largest number of H atoms to be accommodated by the in-core positions.

3.4. Spreading screw dislocation core structure

A spreading core structure can be introduced by further increasing the concentration of hydrogen solutes. When the number of hydrogen atoms is greater than 8, SD core spreading occurs, and the hydrogen atoms occupy the energy-minimum interstitials outside the SD core along two spreading direction. The structure of SD core with 10 H atoms is shown in Fig. 3(c), while other 3 H atoms in the SD core are in the same positions from the view of $[11\bar{1}]$ direction as Fig. 3(b) displayed, so only 7 H atoms could be

(a)

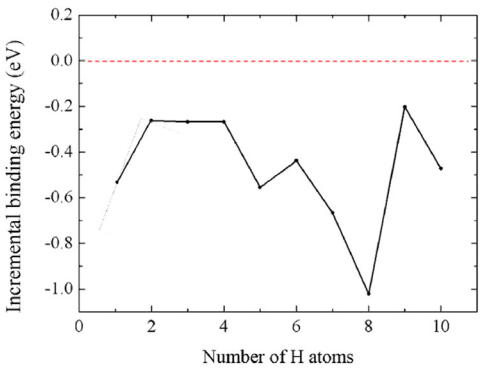

(b)

Number of H atoms	Error(eV)
1	-1.39E-4
2	2.14E-4
3	1.45E-3
4	-5.37E-4
5	-2.54E-4
6	2.13E-4
7	-1.14E-4
8	1.48E-3
9	1.01E-4
10	-1.58E-3

Fig. 2. (a) Incremental binding energy of E^{B}_{SD+H} obtained by the QM/MD simulation. (b) The error from the correction of the binding energy.

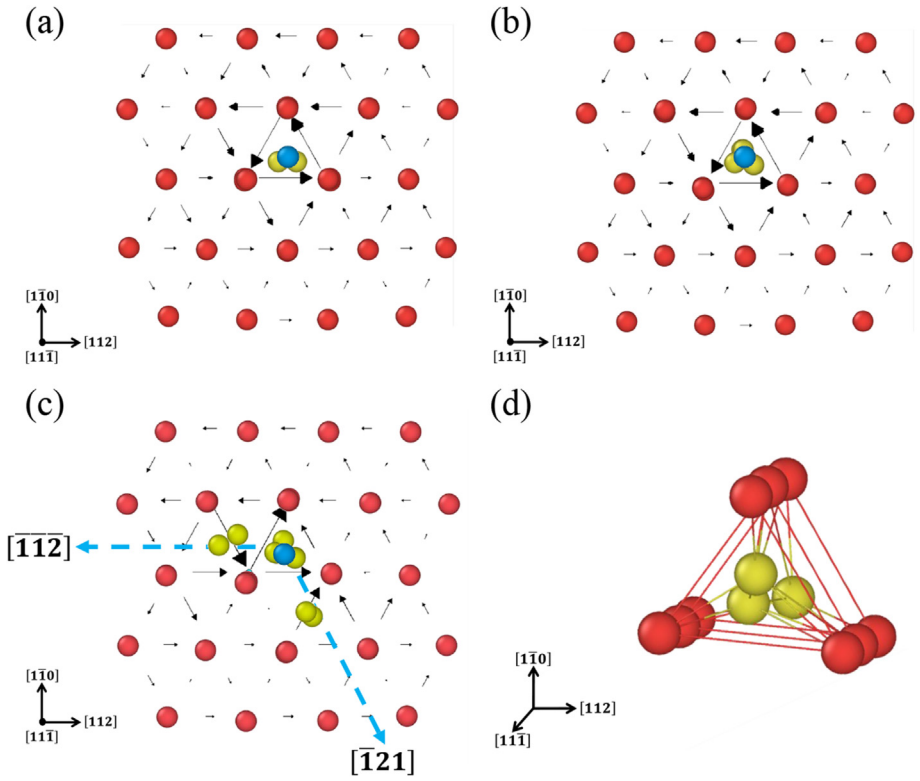

Fig. 3. SD core structures with two hydrogen atoms(a), six hydrogen atoms (b) and ten hydrogen atoms (c) displayed as differential displacement maps (DD map) along the [11$\bar{1}$] direction. W and H atoms are colored by red and yellow, respectively. The initial positions of H atoms are colored in blue to be differentiated. The length of the arrows is proportional to the relative shift of two neighboring atoms along the surface normal after introducing a dislocation into the perfect crystal, where an arrow connecting two neighboring atoms represents a shift of 1/3 Burgers vector b→. (c) The blue dashed arrows are visual guidelines for eyes, representing the expanding direction of the dislocation along the [$\bar{1}$21] and [$\bar{1}\bar{1}$2] directions. (d) The ball-and-stick model of the SD core with 6 hydrogen atoms, visualizing the hydrogen atoms occupying interstitials along the SD line direction. (For interpretation of the references to color in this figure legend, the reader is referred to the Web version of this article.)

observed. This is the first time tungsten SD core spreading induced by a high concentration of interstitial solutes has been investigated, although some DFT studies have focused on the SD core reconstruction in bcc Fe induced by interstitial solutes such as B, C, N, and O [40,41]. More specifically, the dislocation expands along the [$\bar{1}$21] and [$\bar{1}\bar{1}$2] directions unequally, which is similar but not totally identical as an asymmetric degenerated core. The evolution of the dislocation core structure for every cell with a thickness of one Burger's vector along [11$\bar{1}$] direction is displayed in Fig. 4, from bottom (a) to top (d). Although the lengths of the arrows are slightly different in the dislocation core, the spreading of the core could be observed in all the slices. It is obvious that the addition of hydrogen atoms induces a complete change of the entire dislocation sample. The hydrogen atoms do not align along the same line because of the repulsion interaction between them. Instead, four hydrogen atoms occupy two energy-minimum positions along both extension parts of the SD core, while six hydrogen atoms remaining in the SD core maintain the spiral arrangement along the dislocation line. The spreading of the dislocation and the distribution of the hydrogen atoms are mutually influenced. Because the SD core cannot accommodate a high density of hydrogen atoms, the exceeded hydrogen atoms diffused along [$\bar{1}$21] and [$\bar{1}\bar{1}$2] directions, resulting

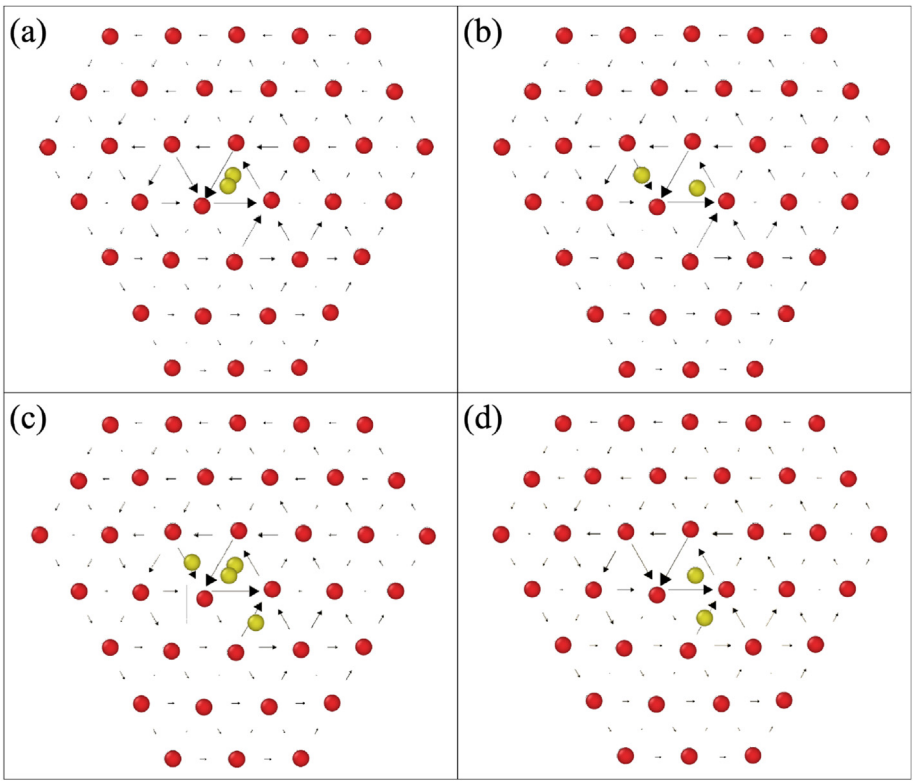

Fig. 4. The differential displacement map for every b thick cell along the [11$\bar{1}$] direction from bottom (a) to top (d) when N = 10. All the colors and symbols have the same meanings as Fig. 3. (For interpretation of the references to color in this figure legend, the reader is referred to the Web version of this article.)

in the extending of the dislocation towards two <112> directions in two {110} planes. Such a preference of hydrogen distribution resembles a field ion microscopy mapped 3D atomic-scale result of carbon distribution around an iron screw dislocation, where carbon atoms in lobe-shaped regions approximately 120° apart are observed [42]. We speculate that lobe-shaped regions and the 120° distribution of C are related to the carbon accumulation preferably along the spreading part of the SD core, while the spreading SD core is resulted from the carbon distribution at the early stage of the carbon diffusing around the SD. Moreover, this transition has an important influence on the dislocation slip plane: the uniform movement of symmetric cores in {110} planes would be observed to be a zigzag path on {112} slip planes with this spreading core structure [20].

The main reason for the core spreading is the H atoms next to the core. Fig. 5(b) displayed the configuration containing a cluster of 4 atoms in the positions next to the dislocation core as Fig. 5(a) shows. The similar core reconstruction effect is observed, while such distribution of H atoms is not decided manually. Without increasing the hydrogen concentration gradually, it is hard to figure out how the "extra" H atoms distribute next to the core, and further the asymmetric spreading of the core. The possibility of the high H concentration in the SD core is estimated according to the mean-field model [20,40,43]. Considering the strongest binding interaction between a hydrogen atom and the dislocation, the hydrogen-dislocation interaction energy is expressed as:

$$E_{int} = E^0_{int} + \triangle E_{easy-spreading} + E_{H-H} \tag{1}$$

where E^0_{int} is the interaction energy of an isolated hydrogen atom with the spreading core, $\triangle E_{easy-spreading}$ is the energetic cost to transform a segment of length b from an easy to a spreading core, and E_{H-H} is the first-neighbor repulsion energy between hydrogen atoms. From our simulations, E_{int} is −0.55eV, and $\triangle E_{easy-spreading}$ is 0.165 eV/b. From Becquart's work, E_{H-H} is 0.47eV [9]. Thus, E^0_{int} is −1.185eV. Then a thermodynamical mean-field model is employed to model the average hydrogen-dislocation interaction energy, which accounts for configurational entropy, but neglects other sources of entropy, vibrational, electronic, and magnetic.

$$E_{int}(c_d) = E^0_{int} + \frac{\triangle E_{easy-spreading}}{c_d} + c_d E_{H-H} \tag{2}$$

where c_d is the average hydrogen concentration on the dislocation core. Minimizing the free energy, the following expression is obtained:

$$\frac{c_d}{1-c_d} = \frac{c_{bulk}}{1-c_{bulk}} exp\left(-\frac{E_{seg}(c_d)}{k_B T}\right) \tag{3}$$

and the segregation energy is as following:

$$E_{seg}(c_d) = E^0_{int} + 2c_d E_{H-H} \tag{4}$$

c_{bulk} represents the hydrogen concentration in the matrix, and it is related to the nominal concentration of hydrogen atoms per tungsten atom, c_{nom}. For a given volume V, the number of hydrogen sites along the dislocation line is $N_d = \rho V/b$, where ρ is the dislocation density. The number of tetrahedral interstitials in the tungsten matrix is $N_0 = 12V/a^3$, where a is the lattice parameter, and there are 12 tetrahedral interstitials in a BCC cell. This gives the following relationship:

$$N_0 c_{bulk} + N_d c_d = N_0 c_{nom}/6 \tag{5}$$

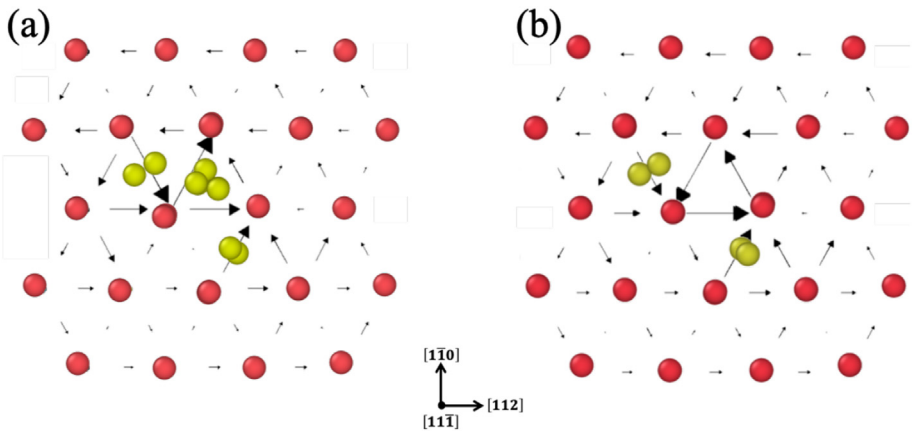

Fig. 5. SD core structures with ten atoms(a) and four hydrogen atoms outside the core(b) displayed as differential displacement maps (DD map) along the [11$\bar{1}$] direction. All the colors and symbols have the same meanings as Fig. 3. (For interpretation of the references to color in this figure legend, the reader is referred to the Web version of this article.)

And 6 means that one tungsten atom is surrounded by 6 tetrahedral interstitials. With these expressions the hydrogen concentration on the dislocation lines corresponding with the dislocation density and the nominal carbon concentration could be obtained.

Fig. 6 gives the temperature dependence of c_d for different nominal concentrations of hydrogen (100 at ppm, 1000 at ppm, 2000 at ppm) and different dislocation density ($10^{15}m^{-2}$, $10^{12}m^{-2}$), respectively. Regarding to the temperature lower than 400 K, the percentage of the hydrogen solutes attracted by the screw dislocation is more than 80% for all nominal concentrations and the dislocation density we considered here, which means that at the dislocation core, the concentration of the hydrogen solutes could be really large, and the high concentration of hydrogen solutes in the core as we discussed in the manuscript is reasonable.

4. Discussion

The spreading behavior of the SD core can be predicted by basic quantities such as the generalized stacking fault energy (γ surface) [44] and increasing edge components [36,44]. The γ surface is based on the energy variation and can be obtained by cutting a crystal along the (110) or (112) planes and displacing the two parts along the [111] direction. Previous studies [14–17] proposed that the core structure is asymmetric if $2\gamma_{b/6} > \gamma_{b/3}$ and otherwise symmetric. Regarding the edge components in the SD core, the degenerate SD core has stronger edge components than the nondegenerate core, which could be revealed by the increase in the normal stress field.

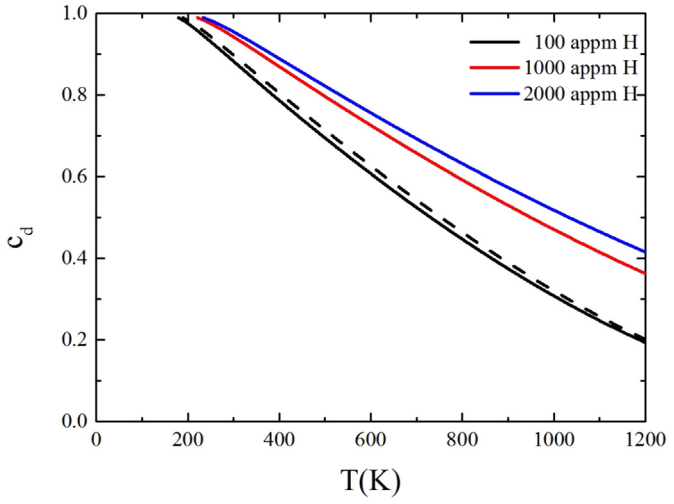

Fig. 6. Temperature dependence of the hydrogen concentration for three nominal concentrations of hydrogen and for two dislocation densities, $10^{15}m^{-2}$ (solid lines) and $10^{12}m^{-2}$ (dashed lines).

4.1. Generalized stacking fault energy (γ surface)

QM method is employed to investigate the change of the γ surface energy of bcc-W induced by H atoms. The simulation box contains 108 atoms on six (112) atomic planes long Y direction. The X, Y, and Z axes of the simulation box are aligned along the [11$\bar{1}$], [1$\bar{1}$0], and [112] directions of the bcc lattice, respectively. A 7.728Å ×26.813Å × 8.254Å bulk (Fig. 7(a)) is proved to be accurate enough for the estimation of stacking fault energy according to the results of the preliminary surface convergence tests. The k-points are chosen as $3 \times 1 \times 3$. The bulk is split into two equal-sized regions along the [1$\bar{1}$0] direction. The upper region is gradually displaced along the [11$\bar{1}$] direction with steps of 0.05b until a total displacement of a full Burgers vector is reached, while the lower region is set rigid. The energy on the γ surface is calculated by $\gamma = \frac{E(u)-E_0}{A}$, where A is the area of the slip plane. The hydrogen atoms are arranged along the [112] direction, presenting as a possible case to work on the hydrogen influence on the γ surface, and are forced to glide together with the upper part of the W bulk. Different numbers of the hydrogen atoms are added to the first nearest tetrahedral interstitial sites above the fixed part. All upper atoms and H atoms are relaxed along [1$\bar{1}$0] and [112] during the simulation.

The gamma surface is plotted for various concentrations of hydrogen during the rigid sliding of the upper (moving) and lower (fixed) part of the crystal along the [11$\bar{1}$] direction, as shown in Fig. 7(b). The (1$\bar{1}$0) γ surface along the [11$\bar{1}$] direction is reduced for increasing hydrogen concentrations, indicating a pronounced reduction in the ideal shear strength. The qualitative shape, however, is insensitive to hydrogen concentration in Fig. 7(c). Hence, the above mentioned criterion, $2\gamma_{b/6} > \gamma_{b/3}$, is not applicable in this case. Thus, the transition observed for the core symmetry is not related to the change in the γ surface shape.

4.2. Stress field analysis

Therefore, the edge components around the SD core are analyzed in symmetric cores and asymmetric cores by investigating

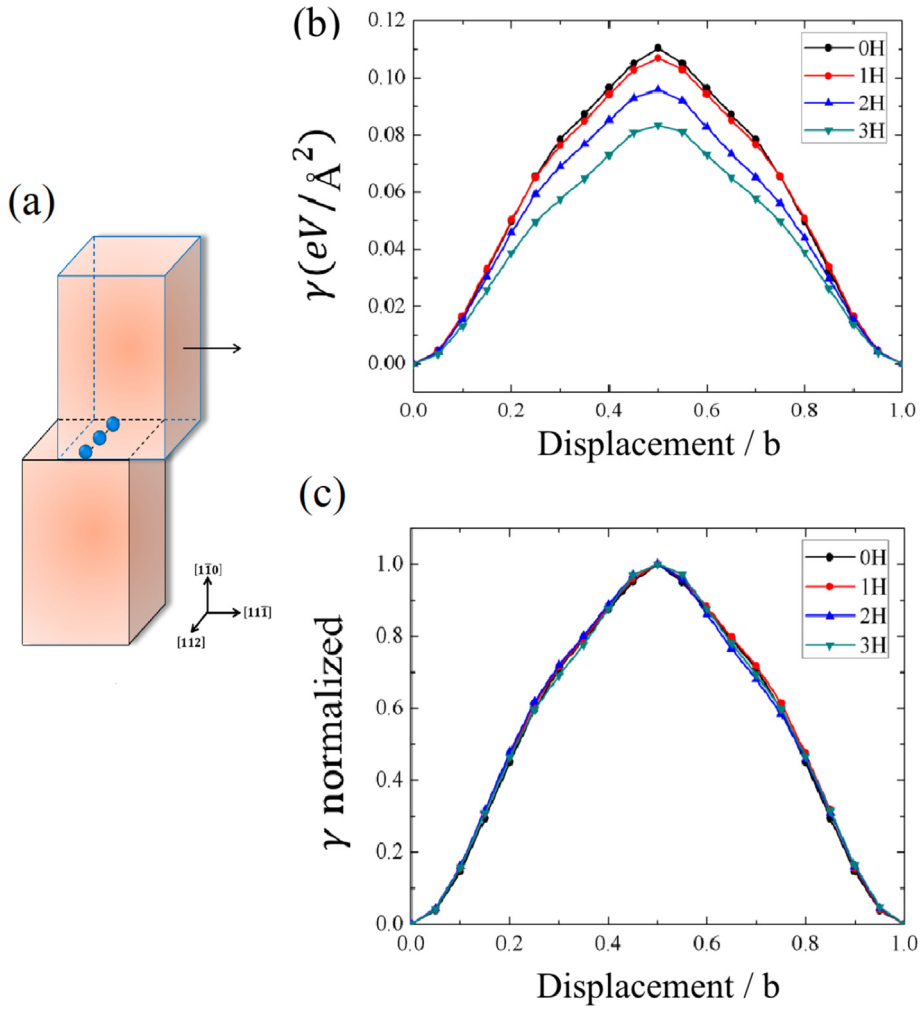

Fig. 7. (a) Schematic plot of the tungsten bulk model employed in the γ surface calculation. This diagram reveals the procedure by which stacking faults are produced, in which the upper part of the atoms are moved along the [11$\bar{1}$] direction in distinct manners. The shearing process is carried out in a supercell consisting of 12 atomic planes in the direction perpendicular to the cut. (b) Illustration of the (1$\bar{1}$0) γ surface along the [11$\bar{1}$] direction for different hydrogen concentrations. In (c), the curves are normalized.

the stress field. When calculating the stress distribution, the hydrogen atoms are removed and the stress distribution is purely decided by the dislocation itself. The dislocation core spreading is introduced by the H clusters, but the different distribution of stresses is resulted from different configuration of the dislocation itself. In previous studies, the characteristics of the stress field were discussed extensively for symmetric and asymmetric cores [16,20,44,45]. The stress fields of the nondegenerate core are $\sigma_r = \sigma_\theta = \sigma_z = 0$, $\tau_{r\theta} = \tau_{rz} = 0$, and $\tau_{z\theta} = Gb/2\pi r$, respectively, for screw dislocations. G stands for the shear modulus, b is the Burger's vector and r is the distance for each atom from the dislocation core. For the spreading asymmetric core, σ_{xx}, σ_{yy} and σ_{zz} are not zero because of the edge components and can be used as indicators of these edge components. The shear stress field of a nondegenerate core with 2 hydrogen atoms is displayed in Fig. 8(a). The shear stress $\tau_{z\theta}$ is symmetric relative to the [11$\bar{1}$] axis and depends only on the distance from the SD core and not on θ for the nondegenerate core. For the shear stress field of the spreading core with 10 hydrogen atoms in Fig. 8(b), the direction of $\tau_{z\theta}$ obviously varies on atom A, and the value of $\tau_{z\theta}$ decreases prominently on atom B, revealing the nonplanar extension associated with the [$\bar{1}\bar{1}$2] direction, and the symmetry of the shear stress no longer exits. The blue arrows indicating the shear stress are for atoms in all layers along Z. Because the shear stress behaves differently along [$\bar{1}\bar{1}$2] and [$\bar{1}$21], the nonplanar extensions are also different from the DD map in Fig. 3(c), where the fractional dislocation extends further along [$\bar{1}\bar{1}$2]. The normal stress σ_{xx} distribution and σ_{yy} distribution of the nondegenerate core are displayed in Fig. 8(c) and (e), which are very low. This distribution of σ_{xx} and σ_{yy} is quite different in the case of a spreading core, with both increasing, as displayed in Fig. 8(d) and (f), respectively. In general, the hydrogen-induced dislocation spreading in the SD core indicates a significant increase of the edge components.

5. Conclusions

To summarize, we have performed QM/MD simulations to characterize the distribution of hydrogen atoms around the cores of SDs along the dislocation line in bcc W. With increasing concentration, the hydrogen atom will display a periodic arrangement and a spiral shape, leading to the spreading of the SD core. The mean-field model is employed to estimate the concentration of the

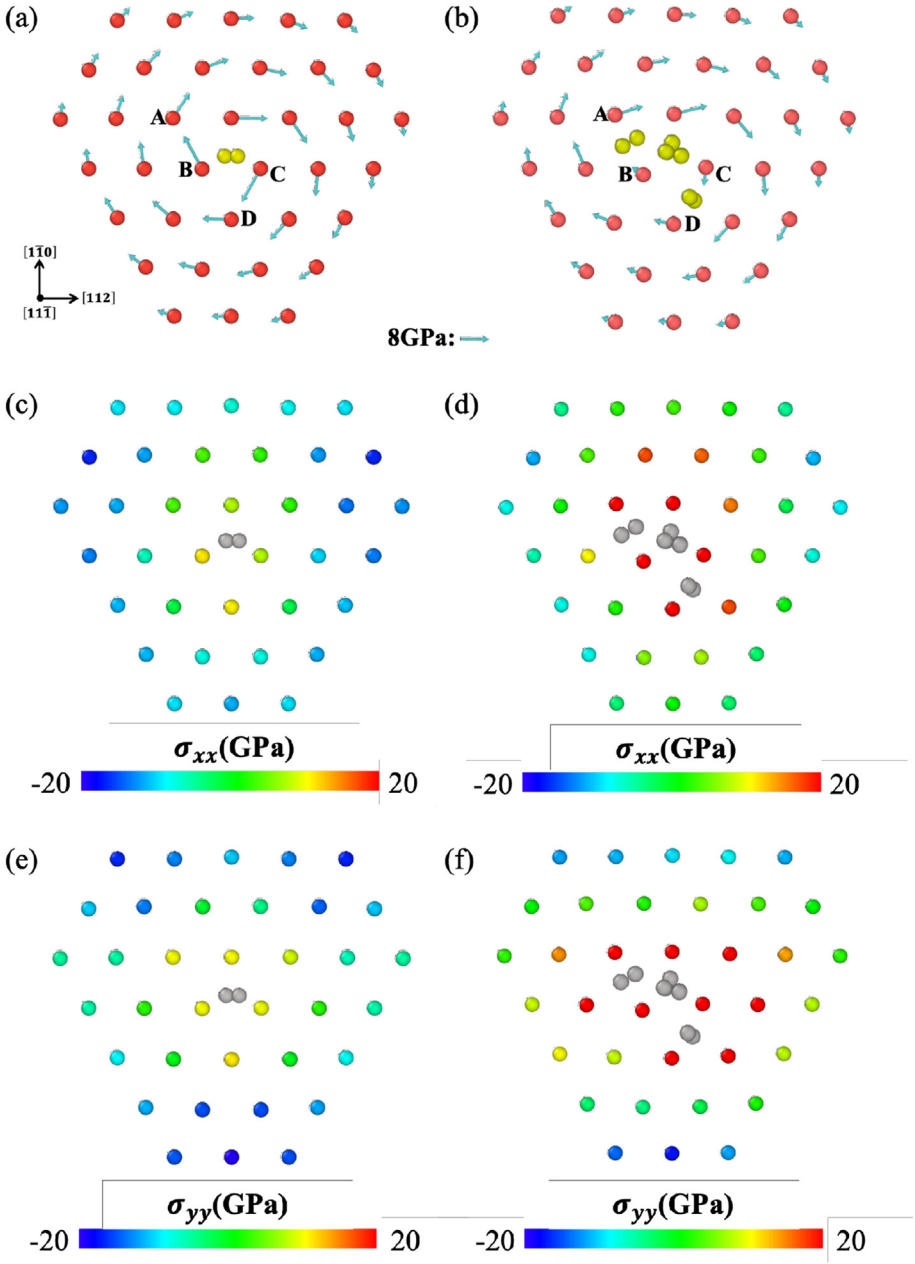

Fig. 8. Shear stress distribution around SD cores with 2 hydrogen atoms (a) and 10 hydrogen atoms(b). W and H atoms are colored red and yellow, respectively. The blue arrows indicate the direction of the shear stress, while the lengths of the arrows are proportional to the relative value of the shear stress $\tau_{z\theta}$. The normal stress along the x direction σ_{xx} of SD cores with 2 hydrogen atoms (c) and 10 hydrogen atoms (d). The tungsten atoms are colored according to the value of σ_{xx}, while the hydrogen atoms are gray for clarity. (e) The normal stress along the y direction σ_{yy} of SD cores with 2 hydrogen atoms and 10 hydrogen atoms (f). The tungsten atoms are colored according to the value of σ_{yy}, while the hydrogen atoms are gray for clarity. (For interpretation of the references to color in this figure legend, the reader is referred to the Web version of this article.)

hydrogen solute in the SD core, revealing that the SD could attract most of the hydrogen solutes, and the high concentration discussed in this work is reasonable. The spreading of the SD core can be attributed to the influence of hydrogen on the stacking fault energy and edge component, as an increase in the number of hydrogen solutes decreases the γ, while the transition from a symmetric core to an asymmetric core arises from the increasing edge components.

Acknowledgement

This work was supported by National Magnetic Confinement Fusion Science Program of China under Grant 2013GB109004 and 2014GB117000, and by National Natural Science Foundation of China under Grant No. 51471092 and No. 11405150.

References

[1] G. Janeschitz, Plasmawall interaction issues in iter, J. Nucl. M. 290–293 (2001) 1–11.
[2] G. Federici, P. Andrew, P. Barabaschi, J. Brooks, R. Doerner, A. Geier, A. Herrmann, G. Janeschitz, K. Krieger, A. Kukushkin, A. Loarte, R. Neu, G. Saibene, M. Shimada, G. Strohmayer, M. Sugihara, Key iter plasma edge and plasmamaterial interaction issues, J. Nucl. M. 313–316 (2003) 11–22, plasma-Surface Interactions in Controlled Fusion Devices 15.
[3] S.J. Zinkle, Fusion materials science: overview of challenges and recent progress, Phys. Plasmas 12 (5) (2005), 058101.
[4] M. Kaufmann, R. Neu, Tungsten as first wall material in fusion devices, Fusion. Eng. Des. 82 (5) (2007) 521–527, proceedings of the 24th Symposium on

Fusion Technology.
[5] Y. Zayachuk, M. t Hoen, P.Z. van Emmichoven, I. Uytdenhouwen, G. van Oost, Deuterium retention in tungsten and tungstentantalum alloys exposed to high-flux deuterium plasmas, Nucl. Fusion 52 (10) (2012) 103021.
[6] O. Ogorodnikova, J. Roth, M. Mayer, Deuterium retention in tungsten in dependence of the surface conditions, J. Nucl. M. 313–316 (2003) 469–477.
[7] V. Alimov, B. Tyburska-Pschel, S. Lindig, Y. Hatano, M. Balden, J. Roth, K. Isobe, M. Matsuyama, T. Yamanishi, Temperature dependence of surface morphology and deuterium retention in polycrystalline iter-grade tungsten exposed to low-energy, high-flux d plasma, J. Nucl. M. 420 (1) (2012) 519–524.
[8] L. Buzi, G.D. Temmerman, B. Unterberg, M. Reinhart, A. Litnovsky, V. Philipps, G.V. Oost, S. Mller, Influence of particle flux density and temperature on surface modifications of tungsten and deuterium retention, J. Nucl. M. 455 (1) (2014) 316–319.
[9] C. Becquart, C. Domain, A density functional theory assessment of the clustering behaviour of he and h in tungsten, J. Nucl. M. 386–388 (2009) 109–111.
[10] V.I. Dubinko, P. Grigorev, A. Bakaev, D. Terentyev, G. van Oost, F. Gao, D.V. Neck, E.E. Zhurkin, Dislocation mechanism of deuterium retention in tungsten under plasma implantation, J. Phys. Condens. Matter 26 (39) (2014) 395001.
[11] D. Terentyev, V. Dubinko, A. Bakaev, Y. Zayachuk, W.V. Renterghem, P. Grigorev, Dislocations mediate hydrogen retention in tungsten, Nucl. Fusion 54 (4) (2014), 042004.
[12] A. Bakaev, P. Grigorev, D. Terentyev, A. Bakaeva, E. Zhurkin, Y.A. Mastrikov, Trapping of hydrogen and helium at dislocations in tungsten: an ab initio study, Nucl. Fusion 57 (12) (2017) 126040.
[13] Y. Zhao, G. Lu, Qm/mm study of dislocation-hydrogen/helium interactions in a-fe, Model. Simul. Mater. Sci. Eng. 19 (6) (2011), 065004.
[14] L. Ventelon, F. Willaime, Core structure and peierls potential of screw dislocations in α-fe from first principles: cluster versus dipole approaches, J. Comput. Mater. Des. 14 (1) (2007) 85–94.
[15] V. Vitek, Core structure of screw dislocations in body-centred cubic metals: relation to symmetry and interatomic bonding, Philos. Mag. A 84 (3–5) (2004) 415–428, https://doi.org/10.1080/14786430310001611644.
[16] C. Woodward, First-principles simulations of dislocation cores, Mater. Sci. Eng. A 400–401 (2005) 59–67. https://doi.org/10.1016/j.msea.2005.03.039. http://www.sciencedirect.com/science/article/pii/S0921509305002686.
[17] S.L. Frederiksen, K.W. Jacobsen, Density functional theory studies of screw dislocation core structures in bcc metals, Philos. Mag. A 83 (3) (2003) 365–375, https://doi.org/10.1080/0141861021000034568. https://doi.org/10.1080/01418610210000345 68.
[18] Y. Wang, Q. Li, C. Li, G. Shu, B. Xu, W. Liu, Dislocation core structures of tungsten with dilute solute hydrogen, J. Nucl. M. 496 (2017) 362–366.
[19] P. Grigorev, D. Terentyev, G. Bonny, E.E. Zhurkin, G.V. Oost, J.-M. Noterdaeme, Interaction of hydrogen with dislocations in tungsten: an atomistic study, J. Nucl. M. 465 (2015) 364–372.
[20] J. P. Hirth, J. Lothe, Theory of Dislocations.
[21] G. Kresse, J. Hafner, Ab initio molecular dynamics for open-shell transition metals, Phys. Rev. B 48 (17) (1993) 13115.
[22] G. Kresse, G. kresse, j. furthmüller, et al., Comput. Mater. Sci. 6 (1996) 15. Comput. Mater. Sci. 6 (1996) 15.
[23] G. Kresse, G. kresse, d. joubert, Phys. Rev. B 59 (1999) 1758. Phys. Rev. B 59 (1999) 1758.
[24] M. Fuchs, M. Scheffler, Ab initio pseudopotentials for electronic structure calculations of poly-atomic systems using density-functional theory, Comput. Phys. Commun. 119 (1) (1999) 67–98.
[25] P. Blöchl, Pe blöchl, phys. rev. b 50 (1994) 17953. Phys. Rev. B 50 (1994) 17953.
[26] H.J. Monkhorst, J.D. Pack, Special points for brillouin-zone integrations, Phys. Rev. B 13 (12) (1976) 5188.
[27] L. F. Wang, X. Shu, G. H. Lu, F. Gao, Embedded-atom method potential for modeling hydrogen and hydrogen-defect interaction in tungsten, Journal of Physics Condensed Matter An Institute of Physics Journal 29 (43).
[28] A. D. Backer, D. R. Mason, C. Domain, D. Nguyen-Manh, M. C. Marinica, L. Ventelon, C. Becquart, S. L. Dudarev, Multiscale modelling of the interaction of hydrogen with interstitial defects and dislocations in bcc tungsten, Nucl. Fusion 58 (1).
[29] S. Plimpton, S. plimpton, J. Comput. Phys. 117 (1995) 1. J. Comput. Phys. 117 (1995) 1.
[30] X. Zhou, H. Wadley, R.A. Johnson, D. Larson, N. Tabat, A. Cerezo, A. Petford-Long, G. Smith, P. Clifton, R. Martens, et al., Atomic scale structure of sputtered metal multilayers, Acta Mater. 49 (19) (2001) 4005–4015.
[31] N. Choly, G. Lu, E. Weinan, E. Kaxiras, Multiscale simulations in simple metals: a density-functional-based methodology, Phys. Rev. B 71 (9) (2005), 094101.
[32] V. Vitek, R. Perrin, D. Bowen, The core structure of 1/2(111) screw dislocations in bcc crystals, Philos. Mag. A 21 (173) (1970) 1049–1073.
[33] A. Stukowski, Visualization and analysis of atomistic simulation data with ovito–the open visualization tool, Model. Simul. Mater. Sci. Eng. 18 (1) (2009), 015012.
[34] L. Ventelon, F. Willaime, E. Clouet, D. Rodney, Ab initio investigation of the peierls potential of screw dislocations in bcc fe and w, Acta Mater. 61 (11) (2013) 3973–3985.
[35] G.D. Samolyuk, Y. Osetsky, R. Stoller, The influence of transition metal solutes on the dislocation core structure and values of the peierls stress and barrier in tungsten, J. Phys. Condens. Matter 25 (2) (2012), 025403.
[36] L. Romaner, C. Ambrosch-Draxl, R. Pippan, Effect of rhenium on the dislocation core structure in tungsten, Phys. Rev. Lett. 104 (2010) 195503, https://doi.org/10.1103/PhysRevLett.104.195503. https://link.aps.org/doi/10.1103/PhysRevLett.104.195503.
[37] S. Ismail-Beigi, T.A. Arias, Ab initio study of screw dislocations in mo and ta: a new picture of plasticity in bcc transition metals, Phys. Rev. Lett. 84 (2000) 1499–1502, https://doi.org/10.1103/PhysRevLett.84.1499. https://link.aps.org/doi/10.1103/PhysRevLett.84.1499.
[38] C. Woodward, S.I. Rao, Flexible ab initio boundary conditions: simulating isolated dislocations in bcc mo and ta, Phys. Rev. Lett. 88 (2002) 216402, https://doi.org/10.1103/PhysRevLett.88.216402. https://link.aps.org/doi/10.1103/PhysRevLett.88.216402.
[39] A. Bakaev, P. Grigorev, D. Terentyev, A. Bakaeva, E. Zhurkin, Y.A. Mastrikov, Trapping of hydrogen and helium at dislocations in tungsten: an ab initio study, Nucl. Fusion 57 (12) (2017) 126040. http://stacks.iop.org/0029-5515/57/i=12/a=126040.
[40] L. Ventelon, B. Lthi, E. Clouet, L. Proville, B. Legrand, D. Rodney, F. Willaime, Dislocation core reconstruction induced by carbon segregation in bcc iron, Phys. Rev. B 91 (22) (2015), 220102(R).
[41] B. Lthi, L. Ventelon, D. Rodney, F. Willaime, Attractive interaction between interstitial solutes and screw dislocations in bcc iron from first principles, Comput. Mater. Sci. 148 (2018) 21–26. https://doi.org/10.1016/j.commatsci.2018.02.016. http://www.sciencedirect.com/science/article/pii/S0927025618300995.
[42] J. Wilde, A. Cerezo, G.D.W. Smith, Three-dimensional atomic-scale mapping of a cottrell atmosphere around a dislocation in iron, Scripta Mater. 43 (1) (2000) 39–48.
[43] G. Trglia, B. Legrand, F. Ducastelle, A. Sal, C. Gallis, I. Meunier, C. Mottet, A. Senhaji, Alloy surfaces: segregation, reconstruction and phase transitions, Comput. Mater. Sci. 15 (2) (1999) 196–235.
[44] M. Duesbery, V. Vitek, Plastic anisotropy in b.c.c. transition metals, Acta Mater. 46 (5) (1998) 1481–1492.
[45] L.V. Azaroff, Crystal lattice defects, Science 14 (6) (1961), 90–90.